Desalination and Water Treatment
www.deswater.com

doi: 10.5004/dwt.2017.21710

100 (2017) 303–310
December

Characterization of hydroxyl radical generation for AOP's treatment on graphite pencil and its NP-modified surfaces

M.A. Morsy

Chemistry Department, King Fahd University of Petroleum & Minerals, Dhahran 31261, Saudi Arabia, Tel. +966138604761, Fax +966138604277, email: mamorsy@kfupm.edu.sa

Received 25 August 2017; Accepted 21 November 2017

ABSTRACT

In this study, an electron paramagnetic resonance/spin trap (EPR/ST) technique was used to investigate hydroxyl radical generation on the surface of NP-modified and unmodified graphite pencil lead. A chemical process was used to modify the graphite flacks on the pencil surfaces with a photoactive titania-nanoparticles (TiOx). The morphology of the graphite surfaces, modified and unmodified, has been investigated by SEM, TEM, XRD spectroscopic techniques. Different types of UV-irradiation light sources indicated that UV-B light source of λ_{max} = 310 nm is the best for the remediation of organic pollutants on the surface of the modified graphite pencil. Moreover, the use of H_2O_2/UV-B/titania-GP combination removes 8 times better the organic contaminants namely, ethylene glycol (EG), than the use of H_2O_2/UV-B/GP system. These results correlate well with the observed oxygen active intermediate trapping experimental results on the modified graphite under the same conditions. It also supports a proposed homolytic fission mechanism of hydrogen peroxide (H_2O_2) that affects directly the advanced oxidation processes (AOPs). These optimum conditions resulted in a faster remediation with a minimal ever reported peroxides for the removal of organic pollutants from a model wastewater.

Keywords: EPR/spin trapping, Graphite pencil, Advanced oxidation processes (AOPs), Nano-metal oxide (Titania), Peroxide oxidation.

1. Introduction

The AOPs using UV/H_2O_2 reaction mixture usually involve the formation of the hydroxyl radical (·OH). These radicals are responsible for the destruction of a range of organic compounds in water [1–5]. Various AOPs have been reported in the literature for the remediation of ethers, including UV/H_2O_2 process [6–10], UV-Fenton and Dark-Fenton [11], ozone and ozone/peroxide [12], also photocatalytic oxidation [13]. However, detailed laboratory studies on the hydroxyl radicals' generation have not been conducted to test hydroxyl radicals' productivity.

The metallic and nonmetallic properties of graphite lead attracted several researchers to propose electrochemical methods by using graphite pencil as working electrodes (PGEs) to quantify a variety of analytes [14–16]. The electrodes have proven to provide high sensitivity, selectivity, and economical tool [17,18]. Modification of lead's surface enhances the detection limit of some biologically active materials to a multi-order magnitude [18,19]. Moreover, graphite and activated carbon were widely utilized to remove organic pollutants from wastewater samples, but via an adsorption process [20,21]. To the best of our knowledge, no AOPs wastewater treatment work has been reported on a surface of a graphite pencil leads or any of its modified forms.

In this work, a simple and inexpensive layer-by-layer (LbL) assembly technique, developed by Decher and co-workers [22,23], was used to prepare a covered micro-structured graphite pencil surface with a deposited TiOx-nano-oxide film. The activities of the modified and

*Corresponding author.

Presented at the Fifth International Conference on Water, Energy and Environment (ICWEE 2017), February 28 – March 2 2017, Sharjah, UAE

unmodified rods toward the AOPs activities have been investigated by EPR/DMPO (5,5-dimethyl-1-pyrroline) spin trap technique. The results show a superior activity of the modified graphite surfaces toward the hydroxyl radical generation compares to the unmodified ones from aqueous/H_2O_2 systems by UV-B light irradiation. They also used to propose a new peroxide hemolytic fission mechanism that postulated the presence of oxygen atom in addition to hydroxyl radical in the AOPs. Moreover, impressive results on the remediation of organic water pollutants, namely ethylene glycol, have been reported.

2. Experimental

2.1. Materials and method of preparations

2.1.1. Spin trapper and EG aqueous sample preparation

The DMPO free radical trapper was obtained from Aldrich–Sigma. Hydrogen peroxide (H_2O_2), 31.4% (without stabilizer), of analytical reagent grade was obtained from Fluka. EG of 99.4% purity, boiling point 55°C, was purchased from Burdick & Jackson, manufactured by Honeywell USA. All solutions were prepared with Milli-Q water. The glassware was rinsed, sequentially with the AlconoxTM cleaning solution, 0.1 M nitric acid, tap water, methanol, and deionized water. Organic systems, ethylene glycol (EG, methanol, and acetone were of HPLC grade and were purchased from Fisher Scientific. A 5% H_2O_2 solution was prepared by diluting 31.4% H_2O_2. An 80 mM DMPO stock solution was freshly prepared for each experiment and kept in the refrigerator during the analysis.

2.1.2. Graphite pencil surface and TiO_2 nano-oxides film preparation

Black pencil leads of types HB were obtained from the local market of Pentel trademark. They are of a 60 mm total length and a 0.5 mm diameter. Their surfaces were oxidized in hot concentrated nitric acid at 100°C for about 5 h, then washed and neutralized with 5 M NaOH solution. The dry neutral-oxidized leads were first immersed in a 1.0 mg/mL poly(diallyl dimethyl ammonium chloride), (PDDA, low MW of 100,000–200,000, 20 wt. % solution in water, from Sigma-Aldrich) for 20 min to render the substrate positively charged, followed by rinsing with DI water twice for 1 min each time and drying with N_2 flow. The pencil rods were then transferred to a 1.0 mg/mL poly(sodium 4-styrene-sulfate), (PSS, C8H7NaO3S, FW 206.2, Typical MW 70,000, 30 wt.% solution in water, from Sigma-Aldrich) for 10 min, rinsed twice with DI water for 1 min each time, and then blown with dry N_2 flow. The PDDA/PSS coating cycle has been repeated seven times to fabricate a multilayer film of superhydrophobic pencil surface.

The deposition of the TiO_2 film on the LbL-coated graphite rod surface was prepared via a hydrothermal method. In this preparation, several positively coated pencil rods were placed in 50 mL aqueous solution of 10–1000 mmoles of titanium(IV) bis (ammonium lactate) dihydroxide (50 wt.% in water, Sigma-Aldrich) solutions in a polytetrafluoroethylene (PTFE) vessel. The PTFE solution vessel was then placed in a stainless steel autoclave reactor (Parr, USA) and kept in the synthetic oven (280A, Fisher Scientific) at 180°C for 24 h. After the completion of the reaction, the pencil rods with the titania coat and some the colloidal titania NP that is centrifuged from the bulk solution were collected for further investigation. All were washed with water, absolute ethanol, acetone, and vacuum-dried at 80°C for 8 h. The dried pencil rods and the collected white solids were calcined at 550°C under a flow of N_2-gas for 4 h.

2.2. Deposited Titania and pencil surface characterization

The diffractograms of the synthesized nanometal oxide were recorded using a Smart Lab X-ray diffractometer (Rigaku, Japan) having Cu-Kα X-rays radiation (λ = 0.15406 nm) source. All the patterns were attained with a diffraction angle (2θ) range of 15–65° at a scan rate of 2°min^{-1}. The pencil surface morphology and the nanostructure of the produced oxides were performed by field emission multimodal electron microscope (LVEM5, Delong, Brno, Czech Republic) that is the only benchtop SEM with the ability to also image in TEM and STEM modes. SEM stub and TEM grid were prepared by putting 1 mm of pencil rods, and 5 µL dilute slurry of the materials onto the special microscope stub and a 400 mesh carbon-coated Cu grid, respectively. After 1 hour of degassing in the spectrometer, the samples were examined.

2.2. Irradiation photochemical reactor setup

Two irradiation procedures were conducted in this study. The first procedure takes place in a Rayonet photochemical reactor (Southern New England Ultraviolet Company, model # PR-100) equipped with a circular array of RPR UV-lamps. The DMPO-H_2O_2 reaction mixtures were placed in Quartz vessel in the photo-reactor for irradiation with unfiltered standard 12 inches, 8-W, RPR-Rayonet fluorescent lamp(s). In the second procedure, the DMPO-H_2O_2 reaction mixture was placed in a standard EPR quartz flat cell (ER 160FC-Q). The mixture was then irradiated by a monochromatic light from a Bausch & Lomb UV-Vis light source equipped with a mercury high source SP 200 and high-intensity monochromator with 1350 groove/mm. During the irradiation period, EPR spectra were taken every 5 min to monitor the formation of the DMPO-radical adducts.

2.3. EPR spectrometer

The electron paramagnetic resonance (EPR) measurements were performed using and SPINSCAN X EPR spectrometer from Adani, Belarus, equipped with a frequency meter, auto-gain, fast registry, and flow flat cell. The spectrometer is operated at the CW X-band and is fully autotuned. The spectrometer parameters were: field sweep width = 335.0 ± 7.0 mT; power = 4 mW; modulation amplitude = 500 mT; microwave power within the range 100–1000 mW. The EPR spectra were recorded at time intervals of 30 s to 15 min of the exposure to a UV-light source of Rayonet.

3. Results and discussion

The hydrothermal treatment of the LbL assembled polymer on the pencil rods produced mechanically durable TiO_2 nanoparticle thin film on the surface of the unmodified HB-pencil rods (Fig. 1a) as captured by a series of high-resolution SEM images presented in Figs. 1c–1g. The TEM microscopic image (Fig. 1b) confirms the uniform distribution of the titania NP and its 5 nm size. Similarly, the SEM images show the generated roughness after the pencil oxidation with nitric acid (Fig. 1d), followed by a LbL-polymerization (Fig. 1e) then solvothermal-titania modification (Fig. 1f) that finally calcined at 550°C to produce the tiny TiO_2 nanoparticles thin-film on the GP-surface of the rods (Fig. 1g).

X-ray diffraction pattern of the synthesized TiO_2 nanoparticles compare to the commercial TiO_2 sample is shown in Fig. 2. The experimental XRD pattern agrees with the JCPDS card no. 075-2546 (anatase TiO_2) and confirming the formation of single phase [24]. The strong diffraction peaks around 2θ position 25° and 48° indicating TiO_2 in the anatase phase. There is no any spurious diffraction peak found in the sample for impurities. Moreover, high intensity of the peaks reflects that the formed TiO_2 NPs are crystalline and narrow diffraction peaks indicate the very small size crystallite.

Testing the activities of pencil rods toward the AOPs required to identify the nature and types of emission nature that could be beneficial out of four standard RPR-Rayonet UV-lamps namely RPR-3500 Å, the RPR-3000 Å, the RPR-2537 Å and RPR-1849/2537 Å. The emission spectra of these lamps are acquired with a Spectra Suite software of Ocean Optic by using a UV-Vis USB2000 spectrometer equipped with a Sony ILX5112048-element linear silicon CCD array detector that provides a measuring range of 200-1100 nm wavelength and 1.0 nm resolution.

The emission spectra indicated that the lamps have different irradiation profile: The RPR-3500 Å and RPR-3000 Å lamps have broad emission bands in the UV-A region (400–316 nm) and the UV-B region (315–281 nm), respectively, while the emission of RPR-2537 Å and RPR-1849/2537 Å lamps produce several sharp emission bands in the UV-C region (280–235 nm) at much shorter wavelengths, starting with a strong band around 254 nm. An early investigation by Spiro and Stigliani [25] of hydroxyl radical generation from aqueous solution indicated that hydroxyl radicals could be formed by the reaction of a water molecule with energetic singlet D-Oxygen atom (1D O) produced by photons having wavelength lower than 310 nm. Thus, RPR-3500 Å lamp should not be used for hydroxyl radical generation

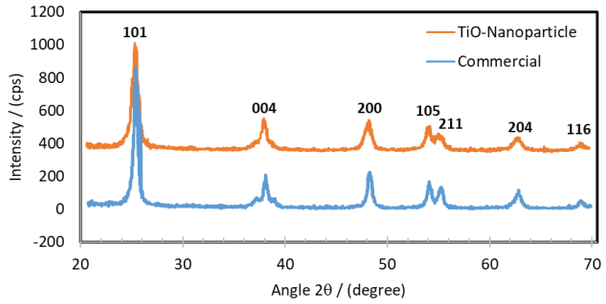

Fig. 2. XRD pattern of synthesized TiO_2 nanoparticles compares to the commercially available titania NPs.

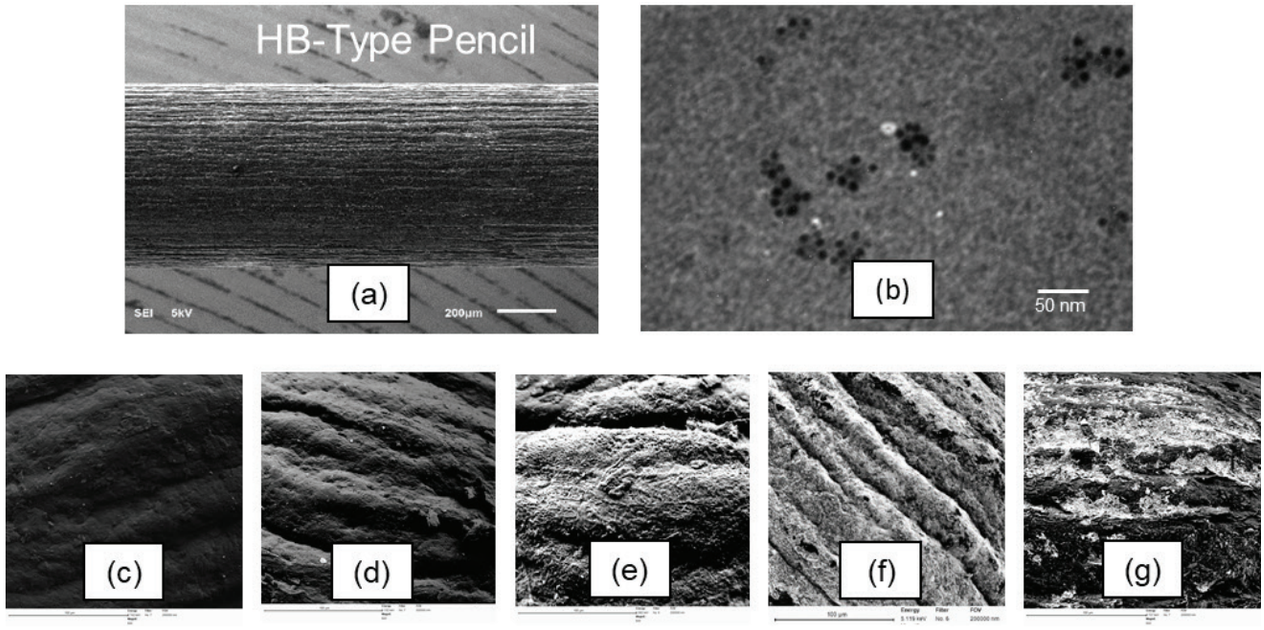

Fig. 1. (a) SEM image of the 0.7 mm HB pencil rod and (b) TEM image of the produced hydrothermal Titania NP confirming the uniform 5 nm diameter size. The high-resolution SEM images of unmodified HB surface (c), HB-HNO_3 oxidized surface (d), HB-LbL polymer treated surface (e), HB- LbL-polymer-TiO_2 solvothermal modified surface (f), and finally the calcined HB-TiO_2 graphite pencil surface at 550°C (g).

from aqueous solution as most of its emitted photons of a lower energy than the amount needed to trigger the process. On the other hand, the RPR-3000 Å lamp and the others produced photons with enough energy that can be used to generate hydroxyl radical from aqueous media. Another important parameter that directly influences the radical generation and their dynamics is the irradiance density per lamp. Table 1 summarizes the values of the irradiance density at every wavelength of the first three lamps.

The energy distribution of the irradiance values in Table 1 agrees well with the emission profile in Fig. 3 where RPR-3000 Å lamp produced the highest irradiance densities at 312 nm wavelength about 52% compare to the PRP-3500 and PRP-2537, which give 32% and 27%, respectively. Further investigations of the lamps activities take place by testing the oxygen (O_2) gas evolution reaction in a 5% peroxide aqueous solutions in a Pyrex tube. The plot of the pressure gas production versus time proves that the formation process is zero order as shown in Fig. 4 supported with images of the evolved gases. The results indicated a superior activity of the RPR-3000 Å lamp compared to other lamps. Moreover, the plot of the slope of the gas production versus the irradiance percent of each lamp at 312 nm gives linear correlation (Fig. 4, in-situ) of a 0.96 correlation coefficient.

In the case of the quartz tubes, still, the UV-B lamp produce the superior results even in the presence of unmodified pencil rods as shown in Fig. 4, bottom graph and image. The observed high production of oxygen gas by the UV-B lamp confirms the irradiation-flux effect of the light source. The glass effect is clear from the observed enhancement of the UV-C production lamp from Pyrex to quartz that could be explained on the basis of the Pyrex cut-off limit of the high energy part of the irradiation. Moreover, the reduction in UV-C compare to UV-B is attributed to a greater oxidation power of UV-C lamps to trigger the self-decay radicals more than gas formation at an earlier time than that observed by UV-B gas formation process. Accordingly, the Pyrex glass and the UV-B source together produced a superior amount of oxygen gases (Fig. 4). The major factors that affect directly the production of the oxygen amount should be the amount of generated radicals as well as their types. Satterfield and Stein [26,27] proposed the following homogeneous dissociation mechanism of hydrogen peroxide (H_2O_2) (Fig. 5):

In the mechanism, two types of radical intermediates were proposed, hydroxyl (OH) and hydrogen-dioxide (HO_2) radicals. Several kinetic investigations have been performed to estimate the hydroxyl radical life time and activation energy of the different processes in the proposed Fig. 5 [28–30]. Although the hydroxyl radicals are the essential intermediate of this process as the most important reactive species, none of the work addressed the presence of the hydrogen-dioxide radical. To point to the formation of radical intermediates in peroxide aqueous solution and provide direct results an exploiting in situ EPR spin trap technique with suitable spin trapper has been conducted. The known efficiency of 5,5-dimethyl-1-pyrroline N-oxide (DMPO) molecule in trapping hydroxyl radical and other short-lived radical species, such as superoxide radical (OOH), methyl radical (CH_3) and many anion radicals [31] make it the spin trapper of choice for this investigation. Fig. 6 shows the nitroxide spin trapped radical(s) of aqueous solutions containing 20 mM DMPO and 200 mM H_2O_2 irradiated with various UV-light sources.

Thus all the three UV-lamps produce a 1:2:2:1 quartet EPR spectrum, peaks 1-4, identical to those of hydroxyl radical (DMPO-OH·) adduct as previously demonstrated [32,33]. The results also confirm the powerful ability the UV-B lamp compared to others to produce the most stable and largest quantity of radicals. On the other hand, another radical species has been observed in the reported spectra of

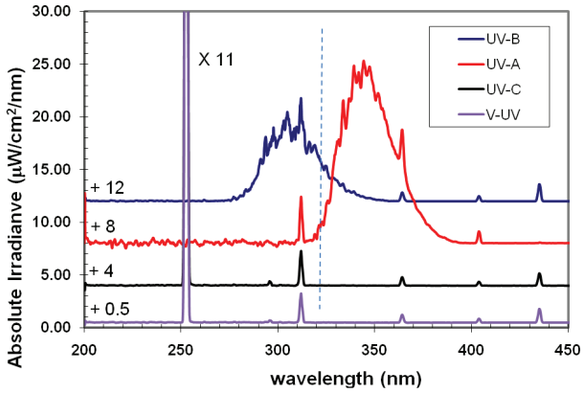

Fig. 3. Emission spectra of the Rayonet UV-A, UV-B, UV-C and V-UV Lamps [added factors were used to split the emission spectra up]. Below the dashed vertical line photons are energetic enough to produce hydroxyl radicals from peroxides [25].

Table 1
Energy distribution of three Rayonet lamps at specific spectral regions. The bold numbers present the highest irradiance per lamp

		Lamp type					
		RPR-3500 (UV-A)		RPR-3000 (UV-B)		RPR-2537 (UV-C)	
Region	Range, nm	Dose, mW m^{-2}	% energy	Dose, mW m^{-2}	% energy	Dose, mW m^{-2}	% energy
UVC	235–280	368	0.67	2049	3.13	75011	88.59
UVB	281–315	3209	2.19	35337	53.94	1673	1.98
UVA	316–400	52670	95.51	20986	32.04	1415	1.67
Visible	401–700	711	1.29	6693	10.22	6108	7.21
NIR	701–850	187	0.34	443	0.68	464	0.55

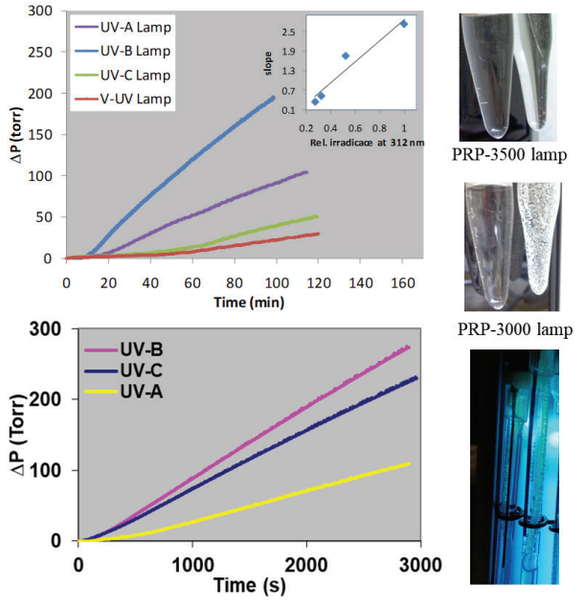

Fig. 4. The gas production of 5% H_2O_2 aqueous solutions in Pyrex tubes using a "Pressure" Measuring Module from PHYWE irradiated with the four types of UV-lamps (Top). In-situ is the plot of the slope of the gas productivity vs. the relative irradiance of the four lamps at 312 nm wavelength. Gas productivity in the irradiated 5% peroxide solutions in quartz tubes with three types of UV-lamps (bottom). On the left-hand side, images of the evolved gases in the different tubes (top and middle of Pyrex and the bottom of quartz).

$$H_2O_2 + M \longrightarrow 2\,{\cdot}OH \mp M^*$$

$$\cdot OH + H_2O_2 \longrightarrow H_2O \mp HO_2^{\bullet}$$

$$HO_2^{\bullet} + H_2O_2 \longrightarrow H_2O \mp O_2 \mp \cdot OH$$

$$2\,HO_2^{\bullet} + M^* \longrightarrow H_2O_2 \mp O_2 \mp M$$

Fig. 5. A homogenous mechanism of hydrogen peroxide dissociation [26,27].

the trapped systems. Detailed investigation of this radical indicated that an atomic oxygen could be also trapped by DMPO to form a DMPO-O· that has been included in the simulated spectrum with a relative concentration 65% of the hydroxyl-DMPO adduct, a_N = 1.524, a_H = 1.500 mT, and 35% of the oxygen-DMPO adduct, a_N = 1.488, a_H = 0.781, $a_{H'}$ = 0.695. This, in turn, accounts for the low quantities of radical-adduct produced when the UV-A or UV-C light irradiation. It is also revealing, for the first time, that cheap Pyrex vessels may be used in place of expensive quartz for the AOPs if a UV-B irradiation is applied and a modified mechanism based on the formation of atomic oxygen can be proposed as shown in Fig. 7.

The EPR spectra in Fig. 8A are a representative sample of the produced radical adducts on the untreated and titania

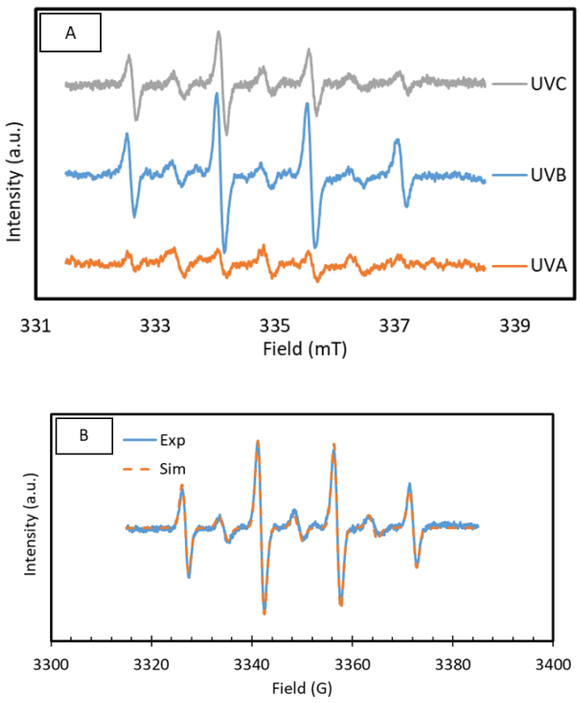

Fig. 6. (A) Experimental EPR spectra of spin trapped oxygenated Radicals of a 20 mM DMPO and 200 mM H_2O_2 irradiated with different UV-Light source and (B) the experimental and simulated spectra of the UVB-light source (λ_{max} = 300 nm, irradiance 10 mW/cm^2; exposure 500 s) and its simulated spectrum by using two nitroxide spin-adducts (relative concentration % 65, a_N = 1.524, a_H = 1.500 mT, g = 2.0052, and % 35, a_N = 1.488, a_H = 0.781, $a_{H'}$ = 0.695, g = 2.0055).

Initiation:

$$H_2O_2 + M \xrightarrow[\lambda < 310\ nm]{h\nu} 2\,{\cdot}OH + M^*$$

Propagation:

$$2\,{\cdot}OH \longrightarrow H_2O + O^{\bullet}$$

$$O^{\bullet} + H_2O \longrightarrow 2\,{\cdot}OH$$

Termination:

$$O^{\bullet} + H_2O_2 \longrightarrow H_2O + O_2$$

$$2\,{\cdot}OH + M^* \longrightarrow H_2O_2 + M$$

Fig. 7. A modified homogeneous mechanism of hydrogen peroxide dissociation using M as reaction quencher, which could be another H_2O_2 molecule, HO_2· radical, or the reaction vessel glass type.

treated HB graphite pencil and their yield during 15 min. These runs were conducted with a homemade photo-reactor equipped with a micro peristaltic pump that is used to continuously pumping the aqueous solution at a 10 rpm to the flat EPR cell for an in situ EPR detection of the produced

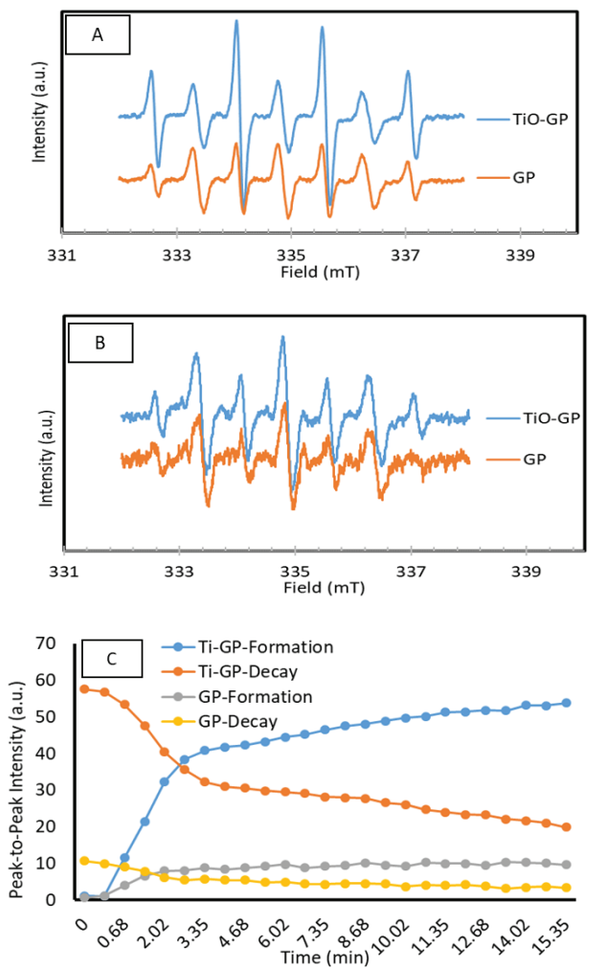

Fig. 8. (A) and (B) EPR spectra of spin trapped oxygenated Radicals of a 15 mM DMPO and 40 mM H_2O_2 and 10 mM DMPO and 10 mM H_2O_2 irradiated with different UV-B light source (λ_{max} = 300 nm, irradiance 20 mW/cm²; exposure 500 s) and (C) the rate of formation and decay of the spin trapped adducts at time intervals 30 s on untreated (GP) and titania treated (Ti-GP) graphite pencil surfaces at 25°C.

adduct radicals. This setup produced a reproducible rate of the adduct formation and decay as presented in Fig. 8C.

The results agree well with the reported photo induced reactivity of TiO_2 toward reactive oxygen radical species production [34–38] and the observed effect of the UV-B light enhancement of the radical production, which was confirmed above by the highest productivity of oxygen gas production as well. This ability is correlated with its high intensity at the 310 nm and thereby produced the largest radical amount compared to both UV-A source (with a less intense 310 nm band) and UV-C source (with the high dynamic that most possibly make the radical be self-scavenger and terminate so early). Therefore, the use of UV-B light source has the additional advantage that the produced hydroxyl radicals will have enough energy and adequately long lifetimes to allow spin trapper is generating the largest quantity of DMPO-radical adducts. The Part B of Fig. 8,

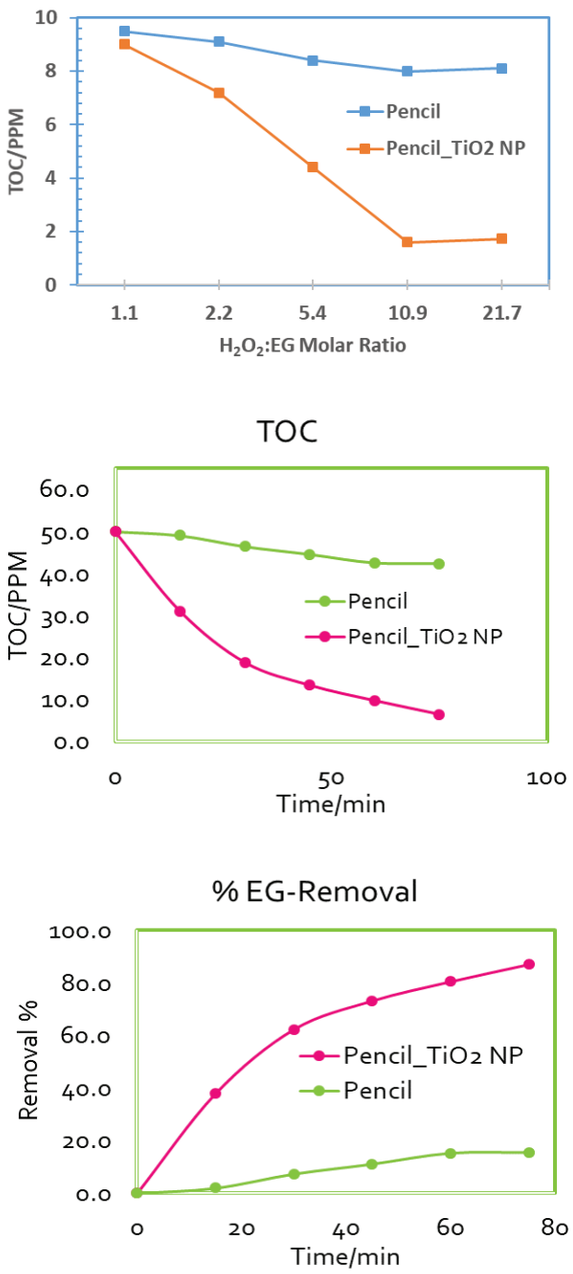

Fig. 9. TOC results of the remediated 10 ppm EG-aqueous solutions at different peroxide ratio (Top) after 60 min UV-B (λ_{max} = 310) irradiation and the rate of 50 ppm EG-aqueous remediation and its percentage removal from a 500 ppm peroxide aqueous solution (bottom) on an untreated (Pencil) and a titania treated (Pencil_TiO_2 NP) graphite pencil surfaces at 25°C.

confirm the continuous generation of the oxygen-DMPO adducts especially by reducing the peroxide concentration which is one of the most active scavengers of this intermediate as proposed in Scheme 2.

Furthermore, preliminary tests on ethylene glycol (EG) removal have been conducted. In these tests, various EG-to-hydrogen peroxide molar ratios, from 1:1 to

1:20 of EG:H_2O_2, in aqueous solutions, were used. The solutions were irradiated in separate experiments by a UV-B light source, λ_{max} = 310 nm, in the presence of the untreated and titania-treated graphite pencils (top graph of Fig. 9). The analysis of the total organic carbon (TOC) takes place by Torch-TOC analyzer, Teledyne Tekmar, USA, based on the combustion and the pressurized CO_2 detection technique. The results indicated that 10 times molar ratio of Peroxide to EG produced the best remediation outcomes. Moreover, the rate analysis of a higher concentration EG-removal, the bottom graphs of Fig. 9 show similar results and confirms the superior remediation of the EG on the surface of the modified graphite pencil (almost 8 times better than the unmodified one, as ~80% removal is obtained on the modified surfaces compare to 10% of the unmodified ones in 60 min UV-B remediation). These results are also in good correlation with the rate of hydrogen peroxide production (Fig. 8) that confirm the dynamics of the hydroxyl radical during the AOP remediation reaction process.

4. Conclusion

The results not only support the current belief that the hydroxyl radical is the essential contributor to AOPs but also introduce a reactive atomic oxygen as another important intermediate in the process. The production efficiency of these reactive oxygen species strongly depends on the UV-regions of the emitted light. The study also shows that the best remediation of the organic pollutants could be achieved by a proper combination of UVB-light source that has emission within 281–315 nm range and the modified graphite carbon surfaces with photocatalytic species via LbL-solvothermal technique. The high selectivity of the trapped reactive oxygen radicals is attributed to their molecular dynamic and lifetime, which are considered to be optimal for a proper chemical reactivity and effective remediation process. Total organic carbon (TOC) analysis confirms the efficiency of the UV-B light-GP system as direct method for the water-organic contaminant content determination. Further work is in progress to optimize for real petrochemical pollutant, model and real wastewater samples especially groundwater ones.

Acknowledgement

Thanks, is due to King Fahd University of Petroleum & Minerals (KFUPM) and The National Science, Technology and Innovation Plan (NSTIP) for financially supporting this work under the research grants 13-WAT250-04. A special appreciation for the quality and proficiency of Mrs. Liliya Bui and her ADANI-Developing Team for being so flexible and so understanding about our needs to create a registry batch commands.

References

[1] R. Andreozzi, V. Caprio, A. Insola, R. Marotta, Advanced oxidation processes (AOP) for water purification and recovery, Catal. Today, 53 (1999) 51–59.

[2] E. Neyens, J.A. Baeyens, Review of classic Fenton's peroxidation as an advanced oxidation technique, J. Hazard. Mater., B98 (2003) 33–50.

[3] K. Ikehata, N.J. Naghashkar, M.C. El-Din, Degradation of aqueous pharmaceuticals by ozonation and advanced oxidation processes: a review, Ozone Sci. Eng., 28 (2006) 353–414.

[4] A.A. Burbano, D.D. Dionysiou, M.T. Suidan, Effect of oxidant-to-substrate ratios on the degradation of MTBE with Fenton reagent, Wat. Res., 42 (2008) 3225–3239.

[5] Y. Deng, R. Zhao, Advanced oxidation processes (AOPs) in wastewater treatment, Wat. Poll., (2015) 167–176.

[6] M.I. Stefan, J. Mack, J.R. Bolton, Degradation pathways during the treatment of methyl tert-butyl ether by the UV/H_2O_2 process, Environ. Sci. Technol., 34 (2000) 650–658.

[7] R.S. Cater, M.I. Stefan, J.R. Bolton, A. Safarzadeh-Amiri, UV/H_2O_2 treatment of methyl-tertbuthyl ether in contaminated water, Environ. Sci. Technol., 34 (2000) 659–662.

[8] M. Pera-Titus, V. Garcia-Molina, M.A. Baños, J. Giménez, S. Esplugas, Degradation of chlorophenols by means of advanced oxidation processes: a general review, Appl. Catal. B: Environ., 47 (2004) 219–256.

[9] B. Tawabini, N. Fayad, M.A. Morsy, The impact of groundwater quality on the removal of methyl tertiary-butyl ether (MTBE) using advanced oxidation technology, Wat. Sci. Tech., 60 (2009) 2161–2165.

[10] M.A. Morsy, Q. Al-Sharari, B.S. El-Tawabini, N.A. Al-Baghli, Electron paramagnetic resonance/spin trapping investigation of hydroxyl radical generation in advanced oxidation processes. '2nd European Conference on Environmental Application of Advanced Oxidation Processes, EAAOP2. Cyprus, September 9–11, 2009.

[11] N. Charton, C. Guilard, C. Hoang-Van, P. Pichat, Products of MTBE degraded in water by photo-Fenton reaction, PSI-Proc., 97 (1997) 65–67.

[12] N.K. Vel Leitner, A.L. Papailhou, J.P. Croue, J. Peyrot, M.. Dore, Oxidation of methyl tert-butyl ether (MTBE) and ethyl tert-butyl ether (ETBE) by ozone and combined ozone/hydrogen peroxide, Ozone Sci. Eng., 16 (1994) 41–54.

[13] R.D. Barreto, K.A. Gray, K. Andre, Photocatalytic degradation of methyl-tert-butyl ether in TiO_2 slurries: a proposed reaction scheme, Wat. Res., 29 (1995) 1243–1248.

[14] J. Wang, A.-N. Kawde, E. Sahlin, Renewable pencil electrodes for highly sensitive stripping potentiometric measurements of DNA and RNA, Analyst, 125(1) (2000) 5–7.

[15] I.G. David, D.E. Popa, M. Buleandra, Pencil Graphite Electrodes: A Versatile Tool in Electroanalysis, J. Analytical Methods in Chemistry (2017). Article ID 1905968, https://doi.org/10.1155/2017/1905968.

[16] M.A. Morsy, A.M. kawde, Electron paramagnetic resonance monitoring for on-demand electrochemically-generated radicals, Electrochim. Acta, 160 (2015) 22–27.

[17] A. Kawde, N. Baig, M. Sajid, Graphite pencil electrodes as electrochemical sensors for environmental analysis: a review of features, developments, and applications, RSC Adv., 6 (2016) 91325–91340.

[18] A. Kawde, M.A. Aziz, Porous copper-modified graphite pencil electrode for the amperometric detection of 4-nitrophenol, Electroanalysis, 26(11) (2014) 2484–2490.

[19] K. Asadpour-Zeynali, P. Najafi-Marandi, Bismuth modified disposable pencil-lead electrode for simultaneous determination of 2-nitrophenol and 4-nitrophenol by net analyte signal standard addition method, Electroanalysis, 23(9) (2011) 2241–2247.

[20] F. Lucking, H. Koser, M. Jank, A. Ritter, Iron powder, graphite and activated carbon as catalysts for the oxidation of 4-chlorophenol with hydrogen peroxide in aqueous solution, Water Res., 32(9) (1998) 2607–2614.

[21] M.A. Anderson, Removal of MTBE and other organic contaminants from water by sorption to high silica zeolites, Environ. Sci. Technol., 34 (2000) 725–727.

[22] G. Decher, J. Hong, Buildup of ultrathin multilayer films by a self-assembly process, 1 consecutive adsorption of anionic and cationic bipolar amphiphiles on charged surfaces, Makromolekulare Chemie. Macromolecular Symposia, 46 (1991) 321–327.

[23] G. Decher, J.B. Schlenoff, Eds. Multilayer Thin Films: Sequential Assembly of Nanocomposite Materials; Wiley-VCH Verlag GmbH & Co.: Weinheim, Germany, 2003.
[24] C. Burda, X. Chen, R. Narayanan, M.A. El-Sayed, Chemistry and Properties of Nanocrystals of Different Shapes, Chem. Rev., 105 (2005) 1025–1102.
[25] T.G. Spiro, W.M. Stigliani, Environmental issues in chemical prespective, SUNY Press 1980.
[26] C.N. Satterfield, T.W. Stein, Homogeneous decomposition of hydrogen peroxide vapor, J. Phys. Chem., 61 (1957) 537–540.
[27] C.N. Satterfield, T.W. Stein, Decomposition of hydrogen peroxide vapor on relatively inert surfaces, Ind. Eng. Chem., 49 (1957) 1173–1180.
[28] P. Attri, Y.U. Kim, D.H. Park, J.H. Park, Y.J. Hong, H.S. Uhm, K.N. Kim, A. Fridman, E.H. Choi, Generation mechanism of hydroxyl radical species and its lifetime prediction during the plasma-initiated ultraviolet (UV) photolysis, Sci. Reports, 5 (2017) 1–8.
[29] J. Weiss, The interaction of OH radicals and of similar free radicals, Trans. Faraday Soc., 36 (1940) 856–861.
[30] P.A. Giguere, I.D. Liu, kinetics of the thermal decomposition of hydrogen peroxide vapor, Can. J. Chem., 35 (1957) 283–293.
[31] P.R. Marriott, M.J. Erkins, D. Griller, Spin trapping for hydroxyl in water: a kinetic evaluation of two popular traps, Can. J. Chem., 58 (1980) 803–807.
[32] H. Utsumi, M. Hakoda, S. Shimbara, H. Nagaoka, Y. Chung, A. Hamada, Active oxygen species generated during chlorination and ozonation, Wat. Sci. Tech., 30 (1994) 91–99.
[33] S.K. Han, K. Ichikawa, H. Utsumi, Quantitative analysis for the enhancement of hydroxyl radical generation by phenols during ozonation of water, Wat. Res., 32 (1998) 3261–3266.
[34] M.A. Grela, M.E.J. Coronel, A.J. Colussi, Quantitative spin-trapping studies of weakly illuminated titanium dioxide sols. Implications for the mechanism of photocatalysis, J. Phys. Chem., 100 (1996) 16940–16946.
[35] C.D. Jaeger, A.J. Bard, Spin trapping and electron spin resonance detection of radical intermediates in the photodecomposition of water at TiO_2 particulate systems, J. Phys. Chem., 83 (1979) 3146–3152.
[36] V. Brezová, D. Dvoranová, A. Staško, Characterization of titanium dioxide photoactivity following the formation of radicals by EPR spectroscopy, Res. Chem. Intermed., 33 (2007) 251–268.
[37] V. Brezová, P. Billik, Z. Vrecková, G. Plesch, Photoinduced formation of reactive oxygen species in suspensions of titania mechanochemically synthesized from $TiCl_4$, J. Mol. Catal. A Chem., 327 (2010) 101–109.
[38] D. Dvoranová, Z. Barbieriková, V. Brezová, Radical Intermediates in Photoinduced Reactions on TiO_2 (An EPR Spin Trapping Study), 19 (2014) 17279–17304.